Macromolecules
ARTICLE

Macromolecules **2009**, *42*, 8817–8826 **8817**
DOI: 10.1021/ma901829d

Regioregular Poly(3-pentylthiophene): Synthesis, Self-Assembly of Nanowires, High-Mobility Field-Effect Transistors, and Efficient Photovoltaic Cells

Pei-Tzu Wu, Hao Xin, Felix Sunjoo Kim, Guoqiang Ren, and Samson A. Jenekhe*

Departments of Chemical Engineering and Chemistry, University of Washington, Seattle, Washington 98195-1750

Received August 17, 2009; Revised Manuscript Received September 25, 2009

ABSTRACT: We report the synthesis, characterization, solution-phase assembly of nanowires, field-effect charge transport, and photovoltaic properties of regioregular poly(3-pentylthiophene) (P3PT), the first regioregular poly(3-alkylthiophene) with an odd-numbered alkyl side chain length to be so investigated. Two samples of P3PT with weight-average molecular weights of 61 800 and 77 000 and 1.4−1.5 polydispersity index have comparable solubility and processability in organic solvents as regioregular poly(3-hexylthiophene) (P3HT) but have a higher melting transition at 259 °C. X-ray diffraction of P3PT films revealed a lamellar structure with an interlayer d_{100} spacing of 1.51 nm and a π-stacking d_{010} spacing of 0.374 nm, both smaller than in P3HT. Crystalline nanowires of 16−17 nm width and aspect ratios as high as 465 were assembled from P3PT solution. Field-effect transistors fabricated from P3PT thin films showed a mobility of holes of up to 0.10 $cm^2/(V\ s)$, and the carrier mobility increased with molecular weight. Bulk heterojunction solar cells based on P3PT/fullerene ($PC_{71}BM$) blend thin films had a power conversion efficiency of 3.70% under 100 mW/cm^2 AM1.5 solar illumination in air and a maximum external quantum efficiency of 69%. Similarly illuminated solar cells based on nanocomposites of P3PT nanowires/$PC_{71}BM$ had a 3.33% power conversion efficiency. These results demonstrate that P3PT is an attractive polymer semiconductor suitable for applications in thin-film and nanowire-based field-effect transistors and bulk heterojunction solar cells.

Introduction

Regioregular poly(3-alkylthiophene)s (P3ATs), exemplified by poly(3-hexylthiophene) (P3HT),[1,2] have been widely studied as p-type semiconductors in organic electronics.[3−9] Virtually all of the P3ATs studied to date have been those with even-numbered alkyl side chains. P3ATs bearing odd-numbered alkyl side chains, C_nH_{2n+1} (n is odd), should also be of fundamental and practical interest because the structural and physical properties of polymers can depend not only on size but also whether n is even or odd.[8−14] The solid-state morphology and charge transport properties of P3ATs are known to be strongly affected by their alkyl side chains.[10−14]

Since the initial reports of improved electronic and optical properties due to their facile self-organization into layered crystalline structures, regioregular P3ATs[3−8] and related derivatives[15,16] have emerged as the most studied, high-mobility p-type polymer semiconductors for device applications in electronics and optoelectronics. In particular, P3HT has been extensively studied as the semiconductor in p-channel organic field-effect transistors (OFETs),[3,4] organic light-emitting diodes,[17] and organic photovoltaic cells (OPV).[5−8] Charge carrier mobilities on the order of 0.1 $cm^2/(V\ s)$ have been reported for P3HT.[4] Bulk heterojunction photovoltaic cells based on blends of P3HT and fullerene, fabricated and processed by various methods, have typical maximum power conversion efficiency (PCE) of 3−5%.[5,6,8]

The thermal properties and solid-state structures of regioregular P3ATs have been studied and correlated with the alkyl chain lengths.[11a,12] The alkyl chain length (n) of the P3ATs is known to play an important role in the crystalline properties and solid-state morphology.[9,11a,12] The thermal properties (T_g, T_m) and optical properties of some polymers not only are known to depend on the alkyl chain length but also can exhibit the odd−even effect.[18] In the lamellar crystalline structure commonly found in the P3ATs, the interlayer distance (d_{100}) is determined by the alkyl chain (C_nH_{2n+1}) length n. For example, the interlayer distance is found to increase from 12.8 to 26 Å when n is even and increases from 4 to 12.[2b,9,11] The role of the alkyl side chain length in even-numbered P3ATs (n = 4−12) in OFETs has been systematically examined.[9,10] It was found that the alkyl side chains in P3AT films act as insulators that interfere with interchain hopping of charge carriers, and thus the longer the alkyl side chain, the lower the hole mobility.[9,10] The effect of the alkyl chain length (n = 4, 6, 8, 10, 12) of P3ATs on the photovoltaic properties of P3AT/fullerene solar cells has also been investigated.[7] P3HT, with hexyl side chains, was found to have the highest efficiency, which was superior by an order of magnitude.[7] We note that the electronic and optical properties, including the field-effect charge transport and photovoltaic properties of a regioregular P3AT with any odd-numbered alkyl side chain length (C_nH_{2n+1}, n is odd), have not been reported. Although a large selection of P3ATs including poly(3-pentylthiophene) (P3PT) are commercially available from Rieke Metals Inc., the synthesis and electronic/optoelectronic properties of P3PT have not been reported.

We report herein the synthesis, characterization, solution-phase self-assembly, photophysics, field-effect charge transport, and photovoltaic properties of regioregular poly(3-pentylthiophene) (P3PT), the first regioregular poly(3-alkylthiophene) having odd-numbered alkyl side chains (C_nH_{2n+1}, n = 5) to be so

*Author for all correspondence. E-mail: jenekhe@u.washington.edu.

Published on Web 10/26/2009

Scheme 1. Synthesis of Regioregular Poly(3-pentylthiophene)

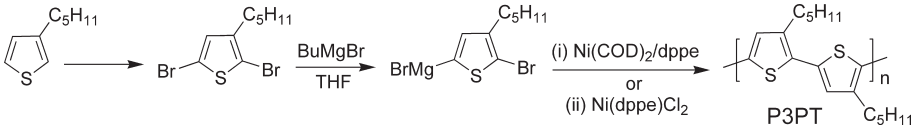

investigated. By using different catalysts and ligands in the polymerization of 2,5-dibromo-3-pentylthiophene, two P3PT samples with significantly different molecular weights were synthesized for our investigation. A commercially available P3PT sample was also acquired from Rieke Metals Inc. and used to study the molecular weight dependence of field-effect carrier mobility. The commonly observed lamellar crystalline structure in regioregular poly(3-alkylthiophene)s was analyzed by X-ray diffraction of P3PT films and self-assembled nanowires. Bottom-contact field-effect transistors were fabricated and used to evaluate the carrier mobility of holes in P3PT thin films, P3PT nanowires, and P3PT/fullerene blends. Bulk heterojunction solar cells based on P3PT/fullerene blends or P3PT nanowire/fullerene nanocomposites were fabricated and used to study the photovoltaic properties of P3PT. Availability of the results for P3PT, the first regioregular P3AT with an odd-numbered alkyl side chain, allowed evaluation of any odd−even effect on the melting temperature (T_m) and interlayer d_{100} spacing of homologous P3AT series.

Results and Discussion

Synthesis of Regioregular Poly(3-pentylthiophene). Surprisingly, the synthesis of P3PT has not been reported. Therefore, we have adapted a literature method (Grignard metathesis polymerization)[1d] for the synthesis of P3HT to prepare two samples of regioregular poly(3-pentylthiophene) (P3PT-1 and P3PT-2) for our investigation (Scheme 1). A difference in the synthesis of P3PT-1 and P3PT-2 is the use of different Ni catalysts and different ligands. By using bis(1,5-cyclooctadiene)nickel(0) [$Ni(COD)_2$] as catalyst and 1,2-bis(diphenylphosphine)ethane (dppe) as ligand in the polymerization of 2,5-dibromo-3-pentylthiophene,[19] we obtained a higher molecular weight polymer, P3PT-1. In contrast, [1,2-bis(diphenylphosphine)ethane]dichloronickel [$Ni(dppe)_2Cl_2$] as catalyst gave a slightly lower molecular weight polymer, P3PT-2. To eliminate any bromine end groups from P3PT, we carried out an end-capping reaction by treating the purified P3PT sample in tetrahydrofuran with methylmagnesium bromide, followed by coupling with CH_3I in the presence of $Ni(dppe)_2Cl_2$ as catalyst.[19] About half of each sample of P3PT was end-capped with a methyl group, resulting in two related samples we labeled as P3PT-1e and P2PT-2e. All the P3PT samples were soluble in organic solvents such as chloroform, chlorobenzene, and 1,2-dichlorobenzene.

The number-average (M_n) and weight-average (M_w) molecular weights, determined by gel permeation chromatography (GPC) relative to polystyrene standards, were 54 000 and 77 000 g/mol, respectively, for P3PT-1. Similarly, P3PT-2 had a M_n of 40 600 g/mol and a M_w of 61 800 g/mol. A commercial poly(3-pentylthiophene) sample ($P3PT^{RM}$), purchased from Rieke Metals Inc., was similarly determined by GPC analysis to have a M_w of 50 400 g/mol with a PDI of 1.6. The head-to-tail regioregularity of the P3PT samples, determined from the ^1H NMR spectra (Figure S1), was 94.3% for P3PT-1 and 94.0% for P3PT-2. The observed 1.4−1.5 polydispersity in the molecular weight of these P3PT samples is comparable to those reported for the even-numbered P3ATs such as P3HT.[1,2]

Differential scanning calorimetry (DSC) scans (Figure S2) of the P3PT samples showed a melting transition with a peak at 259.1 °C for P3PT-1 and 258.5 °C for P3PT-2. In contrast, P3HT and P3BT have reported melting transition temperatures (T_m) at 240−245 and 272 °C, respectively.[12] The observed melting transition temperatures in the family of regioregular poly(3-alkylthiophene)s follow a linear trend, with T_m decreasing with increasing alkyl side chain length as shown in Figure 1. The melting temperature of P3PT is seen to fit the linear dependence of T_m with alkyl chain length n. Thus, our results suggest that the often observed odd−even effect in the melt transition of homologous polymers[18] appears to be absent in the P3ATs. The glass transition temperature (T_g) of P3PT was determined from second DSC scan to be 37 °C, which is to be compared to a higher T_g of 66.9 °C reported for P3BT[11a] and a lower T_g of 12.1 °C reported for P3HT.[20]

We performed X-ray diffraction (XRD) analysis to investigate the packing structure in P3PT films. Figure 2A shows the XRD spectrum of a solution cast P3PT-1 film on a Si substrate. Strong diffraction peaks at $2\theta = 5.9°$ (100), 11.7° (200), and 17.5° (300) are seen in the XRD spectrum. The (100) reflection corresponds to an interlayer d_{100} spacing of 15.1 Å. The XRD results reveal a high degree of crystallinity in P3PT films and suggest a lamellar packing structure on the Si substrate, similar to P3HT films.[3b,6,9] The interlayer stacking of P3PT chains in the solid state is illustrated in Scheme 2, defining d_{100}. The observed interlayer distance (d_{100}) of 15.1 Å in P3PT falls between the d_{100} values of P3BT (12.6 Å)[2b] and P3HT (16.4 Å)[2b] as expected. The interlayer d_{100} spacing is determined by the side-chain length, and it increases with increasing alkyl chain length in P3ATs as seen in Figure 2B.[2b,9,11b] The weak fourth diffraction peak at $2\theta = 23.9°$ can be assigned to both (010) and (400). The (010) reflection corresponds to the $\pi-\pi$ stacking distance (d_{010}) of 3.74 Å in the P3PT films. The observed $\pi-\pi$ stacking distance (d_{010}) in P3PT is very close to that observed in P3HT (3.8 Å),[11b] which is in line with expectation since the linear alkyl side chain length does not have a significant effect on π-stacking of P3ATs.[11b,12]

Photophysical Properties. The optical absorption spectra of a dilute solution (1.0×10^{-6} M) of P3PT-1 in chloroform and a spin-coated thin film are shown in Figure 3A. In solution, a broad featureless absorption band with a maximum (λ_{max}) at 457 nm is seen, which is characteristic of the polythiophene main chain.[1,2] The absorption spectrum of P3PT-1 thin film has a vibronic structure with a λ_{max} at 562 nm and two shoulders at 532 and 612 nm. The 562 nm peak is assigned to the 0−1 transition while the 612 nm shoulder peak is the 0−0 transition whose intensity is indicative of an interchain-delocalized excitation resulting from strong π-stacking of the polymer chains.[21] The much red-shifted thin-film absorption of regioregular P3PT compared to the corresponding absorption in solution is known to originate from an extended conjugated length and self-organized semicrystalline morphology. The optical band gap (E_g^{opt}) of P3PT estimated from the thin-film absorption edge is 1.9 eV, which is identical with that of P3HT.[2] A structured absorption band with λ_{max} at 556 nm and two shoulders at 526 and 610 nm has also been reported for P3HT thin films.[2]

The intensity of the shoulder at 610 nm becomes more prominent after thermal annealing of P3HT films.[5]

Figure 3B shows the photoluminescence (PL) spectra of a dilute solution and a spin-coated thin film of P3PT-1. The observed bright orange PL emission with a maximum at 578 nm in chloroform solution is to be compared with 570 nm for P3HT in chloroform.[2] The intensity of the red emission from the P3PT-1 thin film is weak, but the broad PL emission spectrum is significantly red-shifted from the solution spectrum. Such a red shift of the thin film PL spectrum from the solution is a well-known consequence of the improved electron delocalization in the solid state or good intermolecular ordering in a semicrystalline conjugated polymer.[22]

Self-Assembly of P3PT Nanowires. Ordered/crystalline nanostructures of π-conjugated polymer semiconductors are currently of broad interest in studies of confinement effects on charge transport[23] and electronic properties[24] as well as for applications in electronics, nanoelectronics, and solar energy conversion devices.[25,26] The solution-phase self-assembly of π-conjugated polymers, such as regioregular poly(3-alkylthiophene)s,[11b,25] poly(benzobisimidazobenzophenanthroline) (BBL),[27] and poly(4-alkylquinoline)s,[28] into crystalline nanostructures is known to greatly depend on the solvent and solubility and thus the alkyl side-chain length. Assemblies of P3PT were prepared in 1,2-dichlorobenzene (ODCB) solutions of various concentrations (6−20 mg/mL) and characterized by transmission electron microscopy (TEM) and wide-angle X-ray diffraction (XRD).

The TEM images of the morphology of P3PT nanowires (NWs) self-assembled at different concentrations in ODCB are shown in Figure 4A−C. The NWs grown at low concentration (6 mg/mL) have an average width of 17.2 ± 1.3 nm and lengths of 3−8 μm, giving aspect ratios of 174−465. Those grown at an intermediate concentration (15 mg/mL) had an average width of 17.0 ± 1.4 nm and aspect ratios of 90−200 (Figure 4B). At the highest concentration (20 mg/mL), the P3PT-1 NWs had an average width of 16.4 ± 1.1 nm, lengths of 1.15−4.0 μm, and thus aspect ratios of 70−244. The P3PT-1 NWs assembled at the lowest concentration clearly have the largest aspect ratios and appear to be more flexible compared to those grown at higher concentrations. Similar solution-phase self-assembly of NWs from P3PT-1e gave very similar results. For example, at 10 and 20 mg/mL P3PT-1e NWs with average widths of 17.0 ± 1.4 and 15.7 ± 1.3 nm, respectively, were obtained with aspect ratios of 70−312 (Figure S3).

XRD scans of P3PT NWs drop-casted on Si substrates confirmed their highly crystalline nature. Figure 4D shows a typical XRD spectrum of a film of P3PT-1 NWs. The observed three reflections can be assigned to the (100), (200), and (300) planes; thus, an interlayer lamellar d_{100} spacing of 15.0 Å can be inferred for the molecular packing of P3PT chains within the NWs. This d_{100} value, which is identical for the molecular packing of P3PT chains in solution-cast films (Figure 2A) and the NWs, is significantly smaller than that in P3HT films (16.4 Å)[2b] and larger than that in P3BT NWs.[25]

The observed dimensions (16−17 nm width and 70−465 aspect ratios) of the P3PT NWs are in a range of fundamental and technological interests. The width in particular is within the exciton diffusion lengths of polymer semiconductors (10−20 nm) and thus of interest for the development of more efficient bulk heterojunction solar cells.[25] The average width (16−17 nm) of the present P3PT NWs is larger than the 8−15 nm average widths of reported poly(3-butylthiophene) (P3BT) NWs,[25] probably because of the differences in

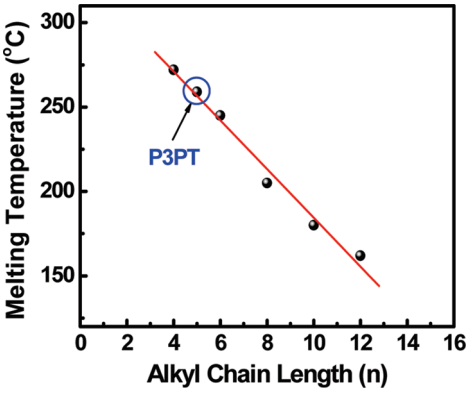

Figure 1. Alkyl chain length dependence of the melting temperatures of regioregular poly(3-alkylthiophene)s for n = 4−12.

Scheme 2. Schematic Interlayer Distance (d_{100}) in P3PT

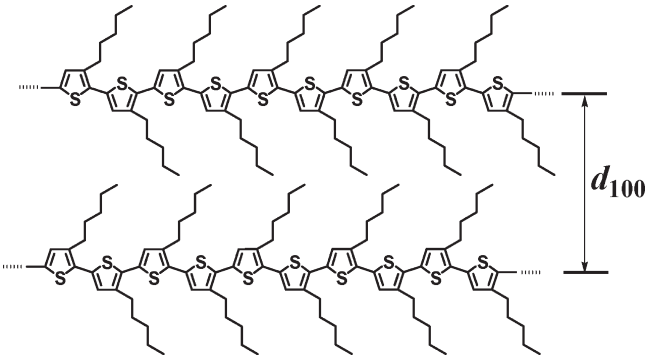

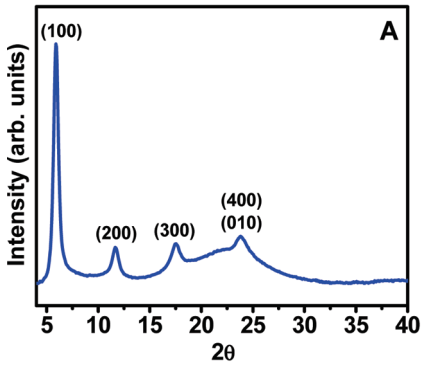

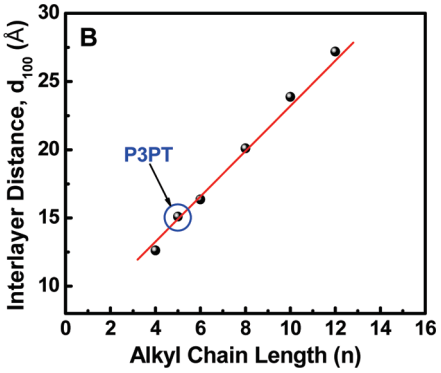

Figure 2. (A) XRD spectrum of a solution cast P3PT-1 film on Si substrate. The interlayer distance, d_{100}, is calculated to be 15.1 Å. (B) Alkyl chain length dependence of the interlayer distance (d_{100}) of regioregular poly(3-alkylthiophene)s for n = 4−12.

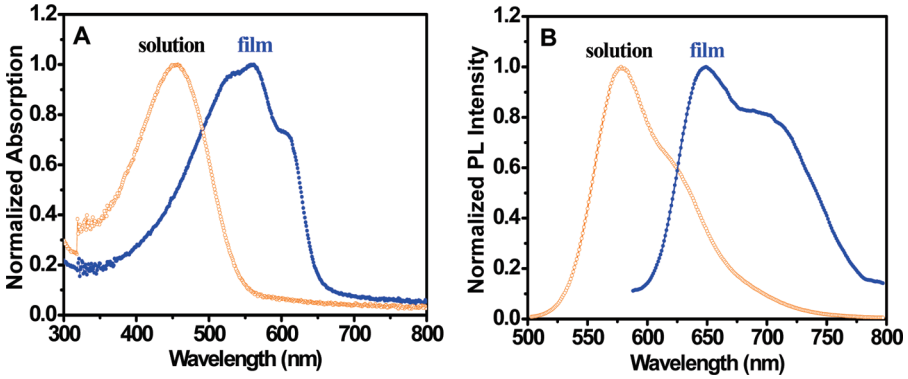

Figure 3. Optical absorption (A) and photoluminescence (B) spectra of P3PT-1 in chloroform solution and as a thin film on glass substrate.

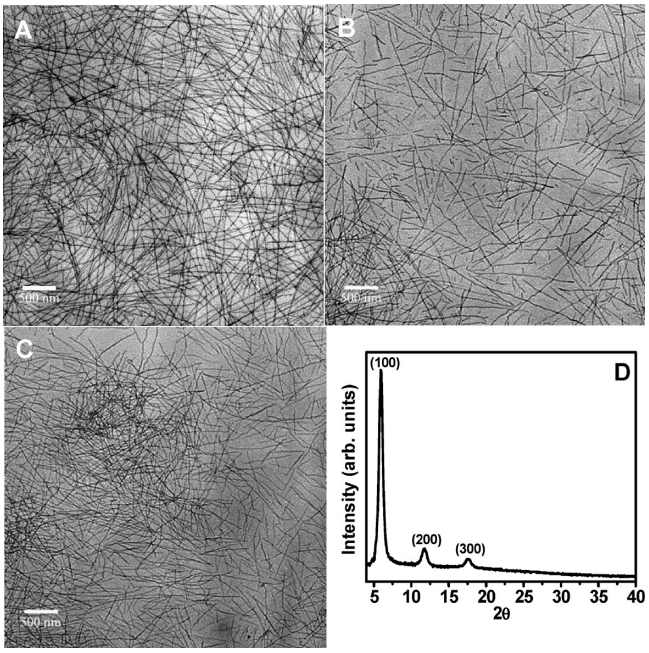

Figure 4. Morphology of P3PT-1 NWs characterized by TEM and XRD. (A) TEM image of P3PT-1 NWs grown at 6 mg/mL. (B) TEM image of P3PT-1 NWs grown at 15 mg/mL. (C) TEM image of P3PT-1 NWs grown at 20 mg/mL. (D) XRD spectrum of P3PT-1 NWs (6 mg/mL) drop-casted on Si substrate.

side-chain length and molecular weight. The molecular weight of our P3PT is much higher than the reported molecular weight of P3BT.[25] Similarly, the reported dimensions of P3HT nanowires (width of 25−50 nm), which are much larger, are to be understood in terms of the different solvents and different molecular weights.[11b,26a] In our laboratory, an attempt to prepare well-defined P3HT nanowires by self-assembly of ODCB solution was made; however, well-defined P3HT nanowires could not be isolated in ODCB solution. On the basis of the width of the NWs, the present P3PT NWs are advantageous for photovoltaic applications since they perfectly match the exciton diffusion length (10−20 nm) of polymer semiconductors.

Field-Effect Transistors. Field-effect charge transport in P3PT was investigated by fabricating and evaluating thin film transistors with gold bottom contacts, n-doped Si gate, and SiO_2 dielectric. Typical OFET output and transfer characteristics are exemplified in Figure 5 for a P3PT-1e thin film device. All the devices showed p-channel transistor characteristics and good current modulation with on/off current ratios of greater than 10^3. The saturation region charge carrier mobility was calculated with the standard equation:[29] $I_{ds} = (\mu_h WC_0/2L)(V_g - V_t)^2$. The square root of the drain current was plotted as a function of gate voltage as shown in Figure 5B, allowing the extraction of the saturation region mobility through the linear fit.[30]

The field-effect transistor parameters are collected in Table 1, including the maximum (μ_h^{max}) and average (μ_h^{avg}) hole mobilities based on 12−18 devices for each sample. The results of OFETs based on a P3PT sample obtained commercially (Rieke Metals) are also shown in Table 1. It is clear that the average mobility of 4.1×10^{-2} $cm^2/(V\ s)$ and maximum mobility of 0.10 $cm^2/(V\ s)$ observed for P3PT-1e mean that charge transport in P3PT is comparable to that in P3HT.[3] The carrier mobility in the end-capped samples is observed to be about 1 order of magnitude higher than those not end-capped (Table 1). A possible explanation for such a dependence is that the bromine end-groups in P3PT-1 and P3PT-2 act as charge traps, limiting charge transport, whereas the end-capped samples (P3PT-1e and P3PT-2e) are free from such traps.

Figure 6 shows the number-average molecular weight (M_n) dependence of the average field-effect carrier mobility in P3PT. Even in the narrow molecular weight range considered here, the average carrier mobility is increased by more than 1 order of magnitude in going from $P3PT^{RM}$ (3.1×10^{-3} $cm^2/(V\ s)$) to P3PT-1e (4.1×10^{-2} $cm^2/(V\ s)$). We note that the polydispersity (PDI) in molecular weight is comparable (1.4−1.6) among the three samples in Figure 6, ruling out the PDI as a factor in the observed carrier mobility trend with M_n. A similar increase of hole mobility (μ_h) with molecular weight of P3HT has been reported and explained in terms of morphological difference in domain boundary structure.[14] The observed increase of μ_h with increasing M_n of P3PT can be understood as a consequence of enhanced interconnectivity between crystalline domains[14a−c] or the presence of tie-crystallites[14d] in thin films of high-molecular-weight polymers. We note that OFETs based on P3PT exhibit a large positive threshold voltage of 52−67 V as shown in Table 1, suggesting oxidative doping of P3PT in ambient air owing to its low ionization potential.

We also estimated field-effect charge transport in the P3PT NWs by spin-coating of a suspension of P3PT-1 NWs onto the channel of the same bottom-contact and bottom-gate OFETs used above to investigate P3PT thin films. Here, the complications include the fact that the coverage of the OFETs channel area is less than 100% and the large number of grain boundary-like interfaces between the network of crystalline NWs. Nevertheless, good output and transfer characteristics can be obtained from the OFETs based on P3PT-1 NWs as shown in Figure 7. On/off current ratios greater than 10^3 were obtained, indicating good

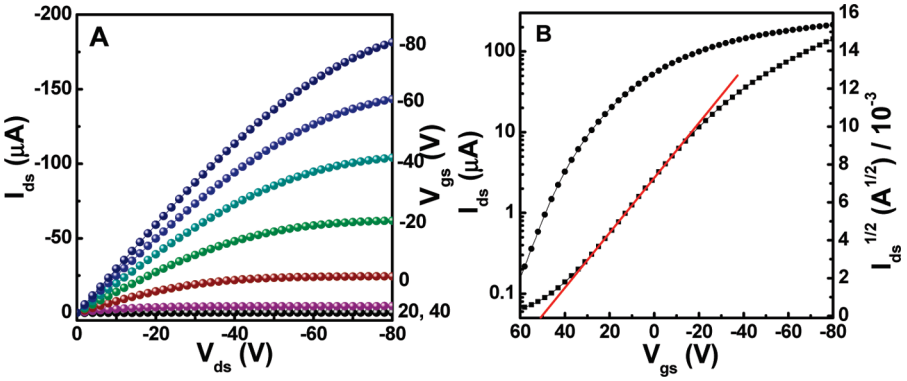

Figure 5. Output (A) and transfer (B) characteristics of a P3PT-1e OFET exhibiting a hole mobility (μ_h) of 0.10 cm^2/(V s).

Table 1. Molecular Weight and Field-Effect Hole Mobility of Poly(3-pentylthiophene)

P3PT samples	M_w	M_n	PDI	μ_h^{max} (cm^2/(V s))	μ_h^{avg} (cm^2/(V s))	$I_{on/off}$	V_t (V)
P3PT-1	77 000	54 000	1.4	3.3×10^{-2}	9.1×10^{-3}	10^3	63
P3PT-1e				0.10	4.1×10^{-2}	10^3	57
P3PT-2	61 800	40 600	1.5	8.8×10^{-3}	7.8×10^{-3}	10^3	67
P3PT-2e				4.8×10^{-2}	1.9×10^{-2}	10^3	52
$P3PT^{RM}$ (Rieke Metals)	50 400	31 800	1.6	7.2×10^{-2}	3.1×10^{-3}	10^3	57

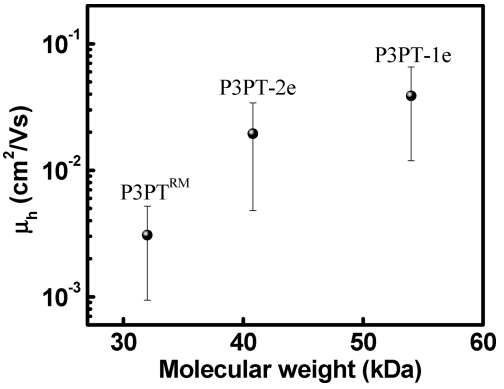

Figure 6. Molecular-weight dependence of field-effect mobility of holes in thin films of P3PT; the sample $P3PT^{RM}$ is from Rieke Metals. The error bar is one standard deviation based on 12−18 devices.

current modulation. Similarly obtained saturation region average and maximum carrier mobilities, without correction for the smaller effective channel area,[23b] were 8.5×10^{-3} and 1.1×10^{-2} cm^2/(V s), respectively, for the self-assembled P3PT-1 NWs. Compared to the P3PT thin film OFETs discussed above, the P3PT-1 NW transistors had a much larger V_t of 75 V. Charge trapping at nanowire/nanowire interfaces can explain the larger V_t value.

Photovoltaic Cells. We have fabricated and evaluated a series of bulk heterojunction (BHJ) solar cells based on P3PT by using the highest molecular weight sample, P3PT-1, including binary blends with $PC_{71}BM$ or $PC_{61}BM$ as well as nanocomposites of P3PT-1 NWs with $PC_{71}BM$ or $PC_{61}BM$. All of the devices were of the basic structure ITO/PEDOT:PSS/blend/LiF/Al and were characterized under AM1.5 solar irradiation in ambient air. The current density−voltage ($J-V$) characteristics of P3PT-1:$PC_{71}BM$, P3PT-1:$PC_{61}BM$, and P3PT-1 NW/$PC_{71}BM$ BHJ solar cells under dark and under 100 mW/cm^2 solar irradiation are shown in Figure 8A. All the devices also showed very good diode properties with rectification ratios higher than 10^3 at ±2 V (not shown). The photovoltaic parameters derived from Figure 8A and similar $J-V$ curves, including the short-circuit current density (J_{sc}), the open-circuit voltage (V_{oc}), the fill factor (FF), and power conversion efficiency (PCE), are collected in Table 2.

The 0.54−0.59 V open-circuit voltages (V_{oc}) observed in the series of P3PT BHJ solar cells are very similar to the 0.5−0.6 V typically seen in solar cells based on P3HT[5,6] or P3BT.[25] The observed similarity in the V_{oc} of P3PT BHJ solar cells to those of P3HT and P3BT is to be expected since the HOMO energy levels of the regioregular P3ATs are similar.[31] The fill factor (FF) of the various P3PT solar cells is in a small range of 0.63−0.69, which is higher than 0.59 seen in P3BT-NW/$PC_{71}BM$ devices[25] and comparable to 0.67 typically observed in the best P3HT:PCBM[6] BHJ devices.

The performance of P3PT BHJ devices based on blends with $PC_{71}BM$ was found to be significantly better compared to $PC_{61}BM$. A power conversion efficiency (PCE) of 3.70% and a photocurrent density of 9.63 mA/cm^2 were achieved in P3PT-1:$PC_{71}BM$ blend devices, whereas 3.05% PCE and J_{sc} of 8.57 mA/cm^2 were obtained in the corresponding $PC_{61}BM$ solar cells. The efficiency (3.33% PCE) and photocurrent of P3PT-1 NW/$PC_{71}BM$ devices were similarly much higher compared to the related $PC_{61}BM$ solar cells (Table 2). A similar enhancement in the performance of $PC_{71}BM$-based BHJ solar cells relative to the $PC_{61}BM$ devices has been observed in other regioregular poly(3-alkylthiophene)s including P3BT[25a] and P3HT.[25a] The improved absorption in P3PT-1:$PC_{71}BM$ blends in the 360−560 nm region compared to the $PC_{61}BM$ blends, as shown in Figure 8B, largely accounts for this enhancement. The absorption spectra of the P3PT-1:fullerene blends show a vibronic structure (Figure 8B) similar to that seen in the pristine P3PT thin films (Figure 3A). In addition to the λ_{max} at 512−520 nm and two shoulders at 557 and 605 nm that are characteristic of P3PT, a distinct peak at 338 nm due to $PC_{61}BM$ or 380 nm due to $PC_{71}BM$ is also observed (Figure 8B). The well-defined shoulder at 605 nm in the absorption spectra of the P3PT/fullerene blends indicates strong π-stacking of the P3PT chains in the blends.

The 1:1 (w/w) P3PT-1:$PC_{71}BM$ blend appears to be the best composition at which the highest efficiency (3.70% PCE) was achieved in the P3PT/fullerene BHJ devices (Table 2). At this composition the P3PT-1:$PC_{71}BM$ BHJ

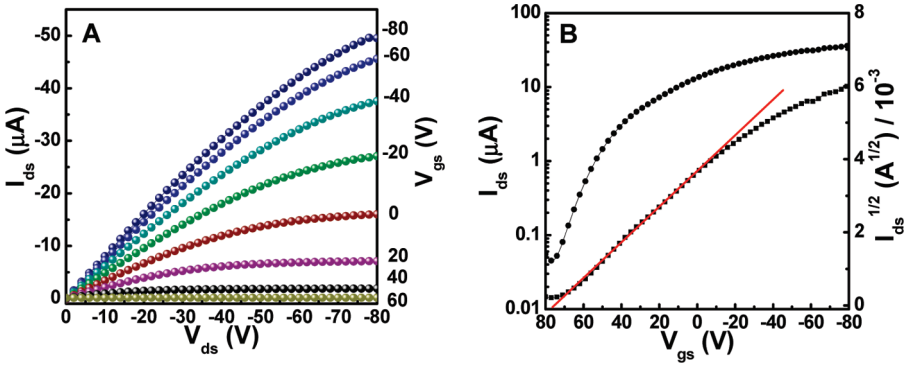

Figure 7. Output (A) and transfer (B) characteristics of an OFET based on P3PT-1 NWs, exhibiting a hole mobility (μ_h) of 0.011 $cm^2/(V\ s)$.

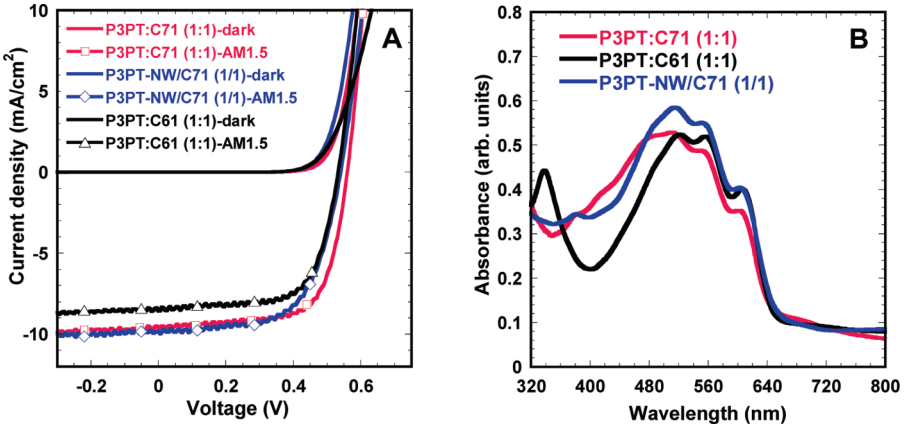

Figure 8. (A) $J-V$ curves of P3PT-1:$PC_{61}BM$ (1:1), P3PT-1:$PC_{71}BM$ (1:1), and P3PT-1 NW/$PC_{71}BM$ (1/1) BHJ solar cells under 100 mW/cm^2 AM1.5 solar irradiation in air. (B) Optical absorption spectra of the same blend thin films in (A).

solar cells combine a high photocurrent (J_{sc} = 9.63 mA/cm^2) with the highest fill factor (FF = 0.69) to achieve the highest efficiency. The efficiency drop to 3.40% PCE along with the photocurrent and the fill factor when the blend composition was 1:0.5 P3PT-1:$PC_{71}BM$ (Table 2). Additional studies of the photovoltaic properties of the P3PT-1/fullerene blends were thus focused primarily on the 1:1 composition. The photoaction or external quantum efficiency (EQE) spectrum of the P3PT-1:$PC_{71}BM$ (1:1) blend solar cell is shown in Figure 9. The photoresponse of the P3PT-1:$PC_{71}BM$ BHJ diode turns on at about 730 nm, and a rather broad peak that centers at ~530 nm is obtained, yielding a maximum EQE of 69% electrons/photon. This EQE value is very similar to those reported for P3HT/fullerene BHJ solar cells.[5]

The light intensity (P) dependence of the photovoltaic properties of P3PT/fullerene BHJ solar cells was investigated to gain some understanding of the loss of charge carriers. The $J_{sc}-V$ characteristics of a P3PT-1:$PC_{71}BM$ (1:1) solar cell under AM1.5 solar irradiation at various light intensities are shown in Figure 10A. The dependence of J_{sc} on irradiation intensity P is shown in Figure 10B, from which a relationship $J_{sc} = 0.22P^{\alpha}$, $\alpha = 0.80$, is found. The nearly linear dependence of the photocurrent on intensity while the open-circuit voltage is nearly constant indicates that no space charge is formed in the active layer,[32] in good agreement with the high fill factor (0.69) observed in the diode at 100 mW/cm^2. The near unity value of the exponent α means that the mechanism of loss of charge carriers in the BHJ device is dominated by monomolecular recombination.[33] We note that an exponent $\alpha = 0.86-0.90$ has been reported for the light intensity dependence of photocurrent density in P3HT:PCBM BHJ devices.[33a]

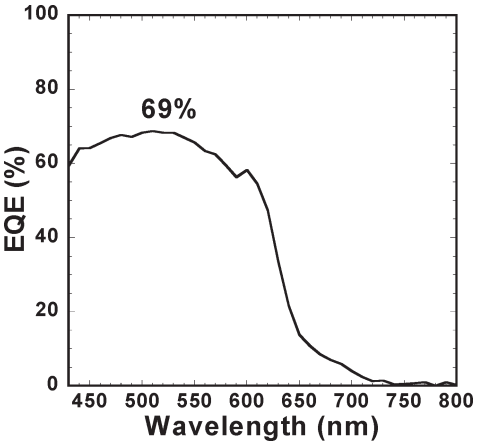

Figure 9. External quantum efficiency (EQE) spectrum of the P3PT-1:$PC_{71}BM$ (1:1) solar cell.

The self-assembled P3PT NWs described above were used to prepare BHJ nanocomposite solar cells. In the case of P3PT-1 NW/$PC_{71}BM$ (1/1) nanocomposite devices, an efficiency of 3.33% PCE with a high photocurrent (J_{sc} = 9.81 mA/cm^2) was achieved even though the film thickness (180 nm) was too high (Table 2). On the other hand, the efficiency (2.62% PCE) of the P3PT-1 NW/$PC_{61}BM$ nanocomposite devices was significantly lower for an active layer thickness of 70 nm. The much larger viscosity of the P3PT-1 NW/fullerene suspensions made controlling and matching the film thickness of the nanocomposite active layers to those of the blends (90 nm) difficult. Nevertheless, the photovoltaic

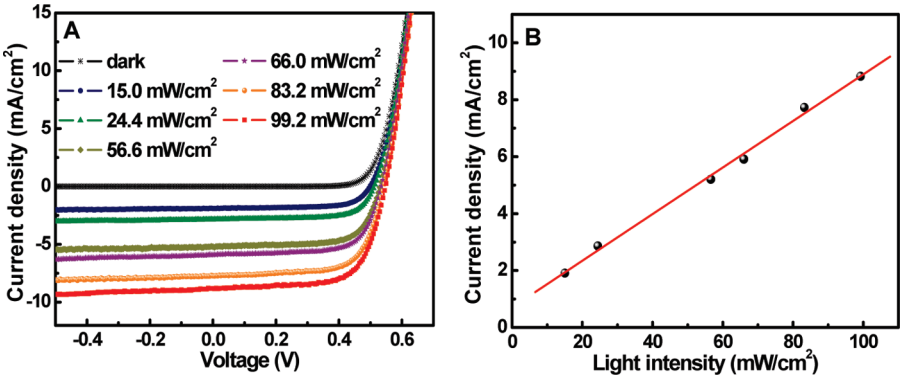

Figure 10. (A) Current density−voltage characteristic of the P3PT-1:$PC_{71}BM$ (1:1) solar cell in the dark and under AM1.5 solar irradiation at various light intensities. (B) Current density of the P3PT-1:$PC_{71}BM$ (1:1) solar cell as a function of the light intensity.

Table 2. Photovoltaic Parameters of P3PT Thin Film and P3PT Nanowire-Based Solar Cells

polymer system[a]	μ_h[b] (cm^2/(V s))	thickness (nm)	J_{sc} (mA/cm^2)	V_{oc} (V)	FF	PCE (%)
P3PT-1:$PC_{61}BM$ (1:1)	2.8×10^{-4}	90	8.57	0.54	0.66	3.05
P3PT-1:$PC_{71}BM$ (1:1)	6.7×10^{-4}	90	9.63	0.56	0.69	3.70
P3PT-1:$PC_{71}BM$ (1:0.5)		90	8.88	0.59	0.65	3.40
P3PT-1 NW/$PC_{61}BM$ (1/1)	2.3×10^{-3}	70	7.19	0.56	0.65	2.62
P3PT-1 NW/$PC_{71}BM$ (1/1)	4.4×10^{-4}	180	9.81	0.54	0.63	3.33

[a] P3PT-1 was used in the fabrication and evaluation of all solar cells. The P3PT-1:fullerene blend devices were spin-coated from solutions (or suspension in the case of P3PT-1 NWs) in 1,2-dichlorobenzene. All spin-coated films were annealed at 160 °C for 10 min. All the solar cells were characterized in ambient air under 100 mW/cm^2 AM1.5 sunlight illumination. [b] Hole mobility was obtained from OFETs based on P3PT-1:fullerene blends or P3PT-1 NW/fullerene nanocomposites.

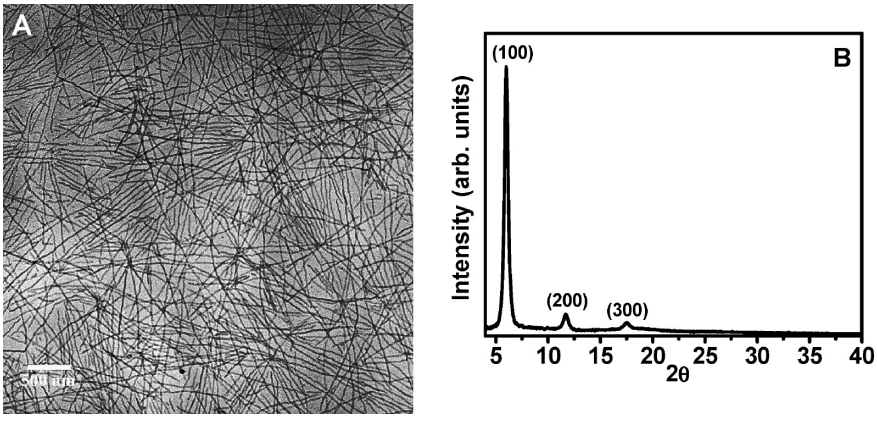

Figure 11. (A) TEM image of the morphology of P3PT-1 NW/$PC_{71}BM$ (1/1) nanocomposite. (B) XRD spectrum of P3PT-1 NW/$PC_{71}BM$ (1/1) nanocomposite drop-casted on Si substrate and annealed at 160 °C for 10 min.

properties of the P3PT nanowire-based BHJ solar cells are very comparable to the blend thin film devices in the case of $PC_{71}BM$ (Table 2). The morphology of the same P3PT-1 NW/$PC_{71}BM$ (1/1) nanocomposites used in solar cells was investigated by TEM imaging and XRD, as shown in Figure 11. The average width of the P3PT-1 NWs in the 1/1 nanocomposites with $PC_{71}BM$ was found to be 15.8 ± 1.4 nm and the aspect ratio was 100−253, which are essentially the same as the dimensions of the pristine P3PT-1 NWs. The XRD spectrum of the P3PT-1 NW/$PC_{71}BM$ (1/1) nanocomposite showed strong (100), (200), and (300) reflections, from which a d_{100} spacing of 15.0 Å is obtained. These results mean that dimensions and crystallinity of the assembled P3PT nanowires are preserved in the BHJ solar cells.

The charge transport in the P3PT-1:fullerene (1:1) BHJ blends and P3PT-1 NW/fullerene (1/1) BHJ nanocomposites were investigated by using the previously described field-effect transistor platform. The average field-effect mobility of holes (μ_h) in films of P3PT-1:$PC_{61}BM$ and P3PT-1:$PC_{71}BM$ blends was 2.8×10^{-4} and 6.7×10^{-4} cm^2/(V s), respectively (Table 2). In the case of P3PT-1 NW/$PC_{61}BM$ and P3PT-1 NW/$PC_{71}BM$ nanocomposites, μ_h was 2.3×10^{-3} and 4.4×10^{-4} cm^2/(V s), respectively. The values of the field-effect mobility of holes are the same order of magnitude for all blends and nanocomposites, except that it is about a factor of 3 higher in P3PT-1 NW/$PC_{61}BM$ nanocomposite films. However, the higher mobility observed in P3PT-1 NW/$PC_{61}BM$ (1/1) nanocompostie films does not translate to improved performance in photovoltaic devices. In fact, there appears to be no correlation between μ_h values and the efficiency of the BHJ solar cells (Table 2). The field-effect mobility of electrons in P3PT:fullerene blends was not observed because our measurements were all done in air.

We have also used the space-charge limited current (SCLC) method to evaluate the charge carrier mobility of holes in the P3PT-1:$PC_{71}BM$ (1:1) blends that showed the best photovoltaic efficiency. The dark-current density (J)−voltage (V) curve for the P3PT-1:$PC_{71}BM$ is shown in

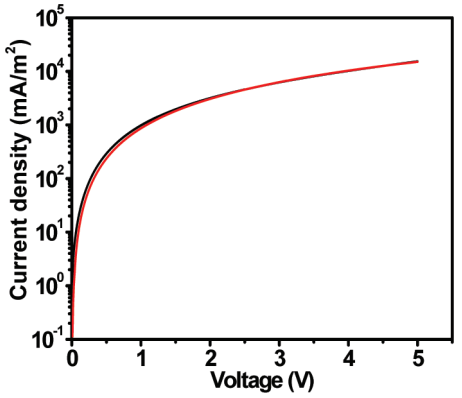

Figure 12. Dark-current density−voltage characteristics of ITO/PEDOT:PSS/P3PT-1:$PC_{71}BM$ (1:1) blend/Au for SCLC measurement of hole mobility. The thickness of the active layer is 86 nm. The black curve is the experimental data, and the red curve represents the fit using a model of single carrier SCL current with field-dependent mobility.

Figure 12 and was analyzed by using the modified Mott−Gurney equation.[34] A zero-field hole mobility of 2.5×10^{-4} $cm^2/(V\ s)$ was obtained. Thus, for the P3PT-1:$PC_{71}BM$ (1:1) blends, hole mobilities obtained from OFET (6.7×10^{-4} $cm^2/(V\ s)$) and SCLC (2.5×10^{-4} $cm^2/(V\ s)$) are the same order of magnitude, confirming good hole transport in the P3PT solar cells. The observed OFET and SCLC mobilities of holes in the present P3PT/fullerene blends are comparable to values reported for P3HT/fullerene BHJ blends that exhibit efficiencies of 4−5% PCE in inert atmosphere measurement.[6]

Conclusions

We have synthesized high molecular weight (M_w = 61 800−77 000 g/mol, PDI = 1.4−1.5) regioregular poly(3-pentylthiophene) (P3PT) and investigated its electronic and optoelectronic properties as well as its self-assembly in solution. P3PT combines good solubility in organic solvents with facile solution-phase self-assembly into crystalline nanowires. P3PT films were found to be highly crystalline, exhibiting a lamellar structure and molecular packing that are characterized by 15.1 Å interlayer d_{100} spacing and 3.74 Å d_{010} π-stacking distance. The P3PT nanowires (NWs) assembled from dichlorobenzene solution had a width of 16−17 nm and aspect ratios of 70−465, depending on the solution concentration. P3PT had an optical band gap of 1.9 eV and thin film absorption spectrum that are almost identical to those of the well-known P3HT.

To demonstrate the potential of P3PT as a p-type semiconductor in organic electronics, we have fabricated and evaluated bottom-contact thin film field-effect transistors and found average and maximum mobility of holes to be 0.04 and 0.10 $cm^2/(V\ s)$, respectively, for the highest molecular weight sample. Bulk heterojunction solar cells based on either P3PT/$PC_{71}BM$ blend thin films or P3PT nanowire/$PC_{71}BM$ thin films were found to have a maximum 3.33−3.70% power conversion efficiency under 100 mW/cm^2 AM1.5 sunlight illumination in ambient air. The similarity of the electronic, optical, and photovoltaic properties of P3PT to those of P3HT when combined with the higher melting temperature and shorter interchain distances of P3PT make regioregular poly(3-pentylthiophene) a promising p-type semiconductor for organic electronics.

Experimental Section

Materials. 3-Pentylthiophene was purchased from TCI Organic, and all other starting materials, reagents, and solvents were purchased from Aldrich; they were used without further purification. For the fabrication of photovoltaic devices, [6,6]-phenyl C_{61}-butyric acid methyl ester ($PC_{61}BM$, 99.5%) and [6,6]-phenyl C_{71}-butyric acid methyl ester ($PC_{71}BM$, >99.0%) were purchased from American Dye Source Inc. and used as received. A commercial poly(3-pentylthiophene) sample ($P3PT^{RM}$) was purchased from Rieke Metals Inc. and used as received.

Preparation of 2,5-Dibromo-3-pentylthiophene. *N*-Bromosuccinimide (NBS) (25.5 g, 143 mmol) was added into the solution of 3-pentylthiophene (10 g, 65 mmol) in DMF/$CHCl_3$ at 0 °C and stirred overnight in the dark. The mixture was poured into water and extracted into ether. The organic layer was evaporated and then purified by silica gel column chromatography with hexane. After purification, a colorless liquid of 2,5-dibromo-3-pentylthiophene was obtained (yield: 19.2 g, 72%.) ^1H NMR ($CDCl_3$): δ (ppm): 6.8 (s, 1H), 2.52 (t, 2H), 1.53 (m, 2H), 1.33 (m, 4H), 0.97 (t, 3H). GC-MS: 312.

Synthesis of Head-to-Tail Regioregular Poly(3-pentylthiophene). *Method 1.* Butylmagnesium chloride (7.49 mL of a 2 M solution in THF, 15 mmol) was added into a solution of 2,5-dibromo-3-pentylthiophene (4.77 g, 15.3 mmol) in anhydrous THF (60 mL) at 10−15 °C and purged with N_2. The solution was degassed and purged upon stirring for 30 min at 10−15 °C and then heated at mild reflux for 1 h. Reflux was stopped before the addition of 1,2-bis(diphenylphosphine)-ethane (103.6 mg, 0.26 mmol) and bis(1,5-cyclooctadiene)-nickel(0) (30.4 mg, 0.1 mmol), and then the mixture was refluxed for at least 24 h. The mixture was cooled to room temperature and poured into methanol to form a precipitate. The precipitate was filtered and washed with methanol and hexane and further purified by Soxhlet extraction in hexane for 2 days. The product was dried in vacuo to give a black solid (yield: 2.07 g, 89%). ^1H NMR ($CDCl_3$), δ (ppm): 6.98 (s, 1H), 2.82 (t, 2H), 1.42 (m, 4H), 0.95 (t, 3H). Regioregularity of this sample (P3PT-1) was estimated to be 94.3%; a weight-average molecular weight (M_w) of 77 000 g/mol with a polydispersity index of 1.4 was determined by gel permeation chromatography (GPC). Estimation of regioregularity was done by integration of the α-methylene protons: A/(A + B), the integral A (range: 2.95−2.65 ppm) and the integral B (range: 2.6625−2.50 ppm).

Method 2. Butylmagnesium chloride (7.45 mL of a 2 M solution in THF, 14.9 mmol) was added into a solution of 2,5-dibromo-3-pentylthiophene (4.65 g, 14.9 mmol) in anhydrous THF (60 mL) at 10−15 °C and purged with N_2. The solution was degassed and purged upon stirring for 30 min at 10−15 °C and then heated at mild reflux for 1 h. Reflux is stopped before the addition of [1,2-bis(diphenylphosphine)ethane]dichloronickel (55 mg, 0.1 mmol), and then the mixture was refluxed for at least 24 h. The mixture was cooled to room temperature and poured into methanol to form a precipitate. The precipitate was filtered and washed with methanol and hexane and further purified by Soxhlet extraction in hexane for 2 days. The product was dried in vacuo to give a black solid (yield: 2.04 g, 90%). ^1H NMR ($CDCl_3$), δ (ppm): 6.98 (s, 1H), 2.82 (t, 2H), 1.42 (m, 4H), 0.95 (t, 3H). Regioregularity of this P3PT-2 sample was estimated to be 94%, and its weight-average molecular weight (M_w) was determined by GPC to be 61 800 g/mol with a polydispersity index of 1.5.

End-Capping Reaction of Poly(3-pentylthiophene). The end-capping of our poly(3-pentylthiophene) samples (P3PT-1 and P3PT-2) was carried out after the purification of the polymers.[19] A P3PT sample (P3PT-1 or P3PT-2) was dissolved into anhydrous THF. An excess amount of methylmagnesium bromide (1 M solution in THF) was added into the mixture to activate and convert the residual bromine end-groups (P3PT-Br) of the polymer into Grignard groups (P3PT-MgBr) and brought to mild reflux for 1 h. The reflux was stopped, and then a catalytic amount of Ni(dppe)Cl_2 was added into the solution. At last, an excess amount of iodomethane was added and refluxed for 2 h. The reaction was quenched with H_2O and precipitated into

methanol. The precipitate was subjected to Soxhlet extraction in hexane and then dried in vacuo to give a black solid. The end-capped polymer samples are termed P3PT-1e and P3PT-2e in relation to their non-end-capped versions.

Solution-Phase Self-Assembly of P3PT Nanowires. All of the self-assembled nanowires in this study were prepared from the high-molecular-weight sample, P3PT-1. A suspension of P3PT-1 in nitrogen-degassed ODCB (6, 15, or 20 mg/mL) was stirred for 24 h at 90−100 °C until P3PT-1 was completely dissolved. The hot solution was filtered through a 0.45 μm filter, and the filtrate was put in a dark environment for 24 h to allow the polymer chains in solution to self-assemble into nanowires. The original orange-brown color of the solution changed to dark violet after P3PT-1 NWs were formed as a dispersion. The P3PT-1 NWs did not dissolve in ODCB by dilution at room temperature, but the nanowires redissolved upon heating to 90−100 °C.

Characterization. ^{1}H NMR spectra were recorded on a Bruker-AF300 spectrometer at 300 MHz. UV−vis absorption spectra were recorded on a Perkin-Elmer model Lambda 900 UV/vis/near-IR spectrophotometer. Spin-coated polymer thin films were prepared from 2 wt % solutions in chloroform. The photoluminescence (PL) emission spectra were obtained with a Photon Technology International (PTI) Inc. model QM-2001-4 spectrofluorimeter. The molecular weights of all polymers were determined by using a Polymer Lab model 220 gel permeation chromatograph (DRI, PL-BV400HT viscometer and PD2040 light scattering) against polystyrene standards in chlorobenzene at 60 °C.

X-ray diffraction spectra were collected on a Bruker D-8 diffractometer with a 4.8 kW TXS Cu rotating anode X-ray source. The incident beam passed through a single Gobel mirror and a 0.5 mm pinhole collimator, creating a focused parallel beam of Cu Kα radiation. The incident angle between the beam and sample was approximately half of the detector angle, and the beam was rastered across a sample area (1 mm × 1 mm) to improve counting statistics. Diffracted radiation was captured with a multiwire area detector, and the collected signal was integrated to give the final plots of intensity vs 2θ. Absolute precision of this diffractometer is within $\pm 0.045°$ of 2θ. The d spacing was calculated from the equation $n\lambda = 2d \sin \theta$.

Transmission Electron Microscopy. The morphology of P3PT-1 NWs and P3PT-1 NW/$PC_{71}BM$ (1/1) nanocomposites was observed by transmission electron microscopy (TEM). TEM images were acquired on a Phillips EM420 microscope operating at 100 kV. The P3PT-1 NW and P3PT-1 NW/$PC_{71}BM$ (1/1) suspension for TEM imaging was diluted 10 times with ODCB (solvent) from the suspension used to fabricate devices. The TEM samples were prepared by dropping a small amount of the diluted P3PT-1 NW/$PC_{71}BM$ nanocomposite suspension onto a TEM grid (400 mesh carbon-coated copper grids, Electron Microscopy Sciences) and allowed to dry in a glovebox overnight.

Fabrication and Characterization of Field-Effect Transistors. Field-effect transistors were fabricated on heavily doped silicon substrates with thermally grown silicon dioxide gate insulator (300 nm). Gold elecrodes (60 nm) with chromium adhesive layer (2 nm) acted as the source and drain electrodes in the bottom-contact/bottom-gate transistors, forming the channel width (W) of 800 μm and length (L) of 20 μm. The substrates were cleaned by ultrasonication with acetone and isopropyl alcohol and purged with argon. Octyltriethoxysilane (OTS-8) monolayer was formed by vapor deposition under vacuum. P3PT solutions in 1,2-dichlorobenzene (ODCB) were deposited on the substrates by spin-coating (2000 rpm, 60 s). The devices were dried in a vacuum at room temperature overnight. Electrical characteristics of the devices were measured on a Keithley 4200 semiconductor characterization system (Keithley Instruments Inc., Cleveland, OH). The field-effect mobility was calculated using the saturation region equation unless otherwise specified. All the measurements were done under dark condition in air.

Fabrication and Characterization of Polymer Photovoltaic Devices. Fullerene solutions (60 mg/mL) were made by dissolving $PC_{61}BM$ or $PC_{71}BM$ in ODCB at 40 °C under stirring and then passing the solution through a 0.2 μm filter. P3PT-1:fullerene ($PC_{61}BM$ or $PC_{71}BM$) blends (1:1, wt/wt) were prepared by mixing 1 mL of P3PT-1 solution (15 mg/mL) with 0.25 mL of fullerene solution (60 mg/mL), whereas the P3PT-1 NW/fullerene ($PC_{61}BM$ or $PC_{71}BM$) nanocomposites were made by mixing a P3PT-1 NW suspension (15 or 6 mg/mL) with the fullerene solution (60 mg/mL) at a weight ratio of 1:1. The P3PT-1 suspensions had a concentration of 24 and 11 mg/mL, respectively. At a spin-coating speed of 1000 rpm, the thickness of a film spin-coated from a 24 mg/mL P3PT-1:fullerene solution was 90 nm. The film thickness of P3PT-1 NW/fullerene nanocomposite films spin-coated from 24 and 11 mg/mL suspensions was 180 and 70 nm, respectively. The P3PT-1 NW/fullerene nanocomposites can be prepared in two ways as described in detail elsewhere for P3BT NWs:[25] (1) mix a suspension of pre-assembled P3PT-1 NWs with the fullerene solution before spin-coating into thin films; (2) the assembly of the P3PT-1 NWs takes place *in situ* in the presence of the fullerene in solution. The photovoltaic cells had an area of 3.57 mm^2 and a structure of ITO/PEDOT/P3PT-1:fullerene/LiF/Al. PEDOT was spin-coated and annealed at 150 °C for 10 min in air, whereas P3PT-1:fullerene active layers were spin-coated at 1000 rpm and annealed at 160 °C for 10 min in a glovebox. Current−voltage characteristics of the solar cells were measured using a HP4155A semiconductor parameter analyzer (Yokogawa Hewlett-Packard, Tokyo). The light intensity of simulated AM1.5 sunlight (100 mW/cm^2) from a filtered Xe lamp was controlled by using a set of neutral density filters. All the characterization steps were carried out under ambient laboratory air. The film thickness was measured by an Alpha-Step 500 profilometer (KLA-Tencor, San Jose, CA).

Acknowledgment. We thank Patrick J. Shamberger and Dr. Fumio S. Ohuchi for the X-ray diffraction analysis and useful discussion. Our work was supported by the Department of Energy Basic Energy Sciences (DE-FG02-07ER46467), the NSF (DMR-0805259 and DMR-0120967), the Office of Naval Research, and in part by the AFOSR EHSS-MURI (FA9550-06-1-0326). Part of this work was conducted at the University of Washington NanoTech User Facility, a member of the NSF National Nanotechnology Infrastructure Network (NNIN).

Supporting Information Available: ^{1}H NMR spectrum, DSC scans, TEM images, and cyclic voltammogram. This material is available free of charge via the Internet at http://pubs.acs.org.

References and Notes

(1) (a) McCullough, R. D.; Lowe, R. D. *J. Chem. Soc., Chem. Commun.* **1992**, 70–72. (b) McCullough, R. D.; Tristram-Nagle, S.; Williams, S. P.; Lowe, R. D.; Jayaraman, M. *J. Am. Chem. Soc.* **1993**, *115*, 4910–4911. (c) McCullough, R. D.; Lowe, R. D.; Jayaraman, M.; Anderson, D. L. *J. Org. Chem.* **1993**, *115*, 904–912. (d) Lowe, R. S.; Khersonsky, S. M.; McCullough, R. D. *Adv. Mater.* **1999**, *11*, 250–253.

(2) (a) Chen, T.-A.; Rieke, R. D. *J. Am. Chem. Soc.* **1992**, *114*, 10087–10088. (b) Chen, T.-A.; Wu, X.; Rieke, R. D. *J. Am. Chem. Soc.* **1995**, *117*, 233–244.

(3) (a) Bao, Z.; Dobabalapur, A.; Lovinger, A. J. *Appl. Phys. Lett.* **1996**, *69*, 4108–4110. (b) Sirringhaus, H.; Brown, P. J.; Friend, R. H.; Nielsen, M. M.; Bechgaard, K.; Langeveld-Voss, B. M. W.; Spiering, A. J. H.; Janssen, R. A. J.; Meijer, E. W.; Herwig, P. T.; de Leeuw, D. M. *Nature* **1999**, *401*, 685–688. (c) Babel, A.; Jenekhe, S. A. *J. Phys. Chem. B* **2003**, *107*, 1749–1754.

(4) Sirringhaus, H.; Tessler, N.; Friend, R. H. *Science* **1998**, *280*, 1741–1744.

(5) (a) Li, G.; Shrotriya, V.; Huang, J. S.; Yao, Y.; Moriarty, T.; Emery, K.; Yang, Y. *Nat. Mater.* **2005**, *4*, 864–868. (b) Ma, W. L.; Yang, C. Y.; Gong, X.; Lee, K.; Heeger, A. J. *Adv. Funct. Mater.* **2005**, *15*, 1617–1622.
(6) Kim, Y.; Cook, S.; Tuladhar, S. M.; Choulis, S. A.; Nelson, J.; Durrant, J. R.; Bradley, D. D. C.; Giles, M.; McCulloch, I.; Ha, C. S.; Ree, M. *Nat. Mater.* **2006**, *5*, 197–203.
(7) (a) Nguyen, L. H.; Hoppe, H.; Erb, T.; Gunes, S.; Gobsch, G.; Sariciftci, N. S. *Adv. Funct. Mater.* **2007**, *17*, 1071–1078. (b) Hiorns, R. C.; de Bettignies, R.; Leroy, J.; Bailly, S.; Firon, M.; Sentein, C.; Khoukh, A.; Preud'homme, H.; Dagron-Lartigau, C. *Adv. Funct. Mater.* **2006**, *16*, 2263–2273.
(8) Campoy-Quiles, M.; Ferenczi, T.; Agostinelli, T.; Etchegoin, P. G.; Kim, Y.; Anthopoulos, T. D.; Stavrinou, P. N.; Bradley, D. D. C.; Nelson, J. *Nat. Mater.* **2008**, *7*, 158–164.
(9) Park, Y. D.; Kim, D. H.; Jang, Y.; Cho, J. H.; Hwang, M.; Lee, H. S.; Lim, J. A.; Cho, K. *Org. Electron.* **2006**, *7*, 514–520.
(10) Babel, A.; Jenekhe, S. A. *Synth. Met.* **2005**, *148*, 169–173.
(11) (a) Yazawa, K.; Inoue, Y.; Yamamoto, T.; Asakawa, N. *Phys. Rev. B* **2006**, *74*, 094204. (b) Samitsu, S.; Shimomura, T.; Heike, S.; Hashizume, T.; Ito, K. *Macromolecules* **2008**, *41*, 8000–8010.
(12) Causin, V.; Marega, C.; Marigo, A.; Valentini, L.; Kenny, J. M. *Macromolecules* **2005**, *38*, 409–415.
(13) Yang, H.; Shin, T. J.; Yang, L.; Cho, K.; Ryu, C. Y.; Bao, Z. *Adv. Funct. Mater.* **2005**, *15*, 671–676.
(14) (a) Zen, A.; Saphiannikova, M.; Neher, D.; Grenzer, J.; Grigorian, S.; Pietsch, U.; Asawapirom, U.; Janietz, S.; Scherf, U.; Lieberwirth, I.; Wegner, G. *Macromolecules* **2006**, *39*, 2162–2171. (b) Kline, R. J.; McGehee, M. D.; Kadnikova, E. N.; Liu, J.; Fréchet, J. M. J.; Toney, M. F. *Macromolecules* **2005**, *38*, 3312–3319. (c) Chang, J.-F.; Clark, J.; Zhao, N.; Sirringhaus, H.; Breiby, D. W.; Andreasen, J. W.; Nielsen, M. M.; Giles, M.; Heeney, M.; McCulloch, I. *Phys. Rev. B* **2006**, *74*, 115318. (d) Brinkmann, M.; Rannou, P. *Macromolecules* **2009**, *42*, 1125–1130. (e) Joshi, S.; Pingel, P.; Grigorian, S.; Panzner, T.; Pietsch, U.; Neher, D.; Forster, M.; Scherf, U. *Macromolecules* **2009**, *42*, 4651–4660. (f) Woo, C. H.; Thompson, B. C.; Kim, B. J.; Toney, M. F.; Fréchet, J. M. J. *J. Am. Chem. Soc.* **2008**, *130*, 16324–16329.
(15) (a) Ong, B. S.; Wu, Y.; Liu, P.; Gardner, S. *J. Am. Chem. Soc.* **2004**, *126*, 3378–3379. (b) Moulé, A. J.; Allard, S.; Kronenberg, N. M.; Tsami, A.; Scherf, U.; Meerholz, K. *J. Phys. Chem. C* **2008**, *112*, 12583–12589. (c) Koppe, M.; Scharber, M.; Brabec, C.; Duffy, W.; Heeney, M.; McCulloch, I. *Adv. Funct. Mater.* **2007**, *17*, 1371–1376.
(16) (a) McCulloch, I.; Heeny, M.; Bailey, C.; Genevicius, K.; MacDonald, I.; Shkunov, M.; Sparrowe, D.; Tierney, S.; Wagner, R.; Zhang, W.; Chabinyc, M. L.; Kline; McGehee, M. D.; Toney, M. F. *Nat. Mater.* **2006**, *5*, 328–333. (b) Miyanishi, S.; Tajima, K.; Hashimoto, K. *Macromolecules* **2009**, *42*, 1610–1618. (c) Sivula, K.; Luscombe, C. K.; Thompson, B. C.; Fréchet, J. M. J. *J. Am. Chem. Soc.* **2006**, *128*, 13988–13989. (d) Shi, C.; Yao, Y.; Yang, Y.; Pei, Q. *J. Am. Chem. Soc.* **2006**, *128*, 8980–8986. (e) Huang, Y.; Wang, Y.; Sang, G.; Zhou, E.; Huo, L.; Liu, Y.; Li, Y. *J. Phys. Chem. B* **2008**, *112*, 13476–13482.
(17) Berggren, M.; Inganäs, O.; Gustafsson, G.; Rasmusson, J.; Andersson, M. R.; Hjertberg, T.; Wennerström, O. *Nature* **1994**, *372*, 444–446.
(18) Egbe, D. A. M.; Ulbricht, C.; Orgis, T.; Carbonnier, B.; Kietzke, T.; Peip, M.; Metzner, M.; Gericke, M.; Birckner, E.; Pakula, T.; Neher, D.; Grummt, U.-W. *Chem. Mater.* **2005**, *17*, 6022–6032.
(19) (a) Heeny, M.; Zhang, W.; Duffy, W.; McCulloch, I.; Koller, G. World Patent Application WO2007/059838, **2007**. (b) McCullough, R. D.; Liu, J.; Ewbank, P. C.; Sheina, E. E. US Patent 6602974, 2003.
(20) Zhao, J.; Swinnen, A.; Van Assche, G.; Manca, J.; Vanderzande, D.; Van Mele, B. *J. Phys. Chem. B* **2009**, *113*, 1587–1591.
(21) Österbacka, R.; An, C. P.; Jiang, X. M.; Vardeny, Z. V. *Science* **2000**, *287*, 839–842.
(22) (a) Brown, P. J.; Thomas, D. S.; Kohler, A.; Wilson, J. S.; Kim, J.-S.; Ramsdale, C. M.; Sirringhaus, H.; Friend, R. H. *Phys. Rev. B* **2003**, *67*, 064203. (b) Jenekhe, S. A.; Osaheni, J. A. *Science* **1994**, *265*, 765–768. (c) Jiang, X.; Österbacka, R.; Korovyanko, O.; An, C. P.; Horovitz, B.; Janssen, R. A. J.; Vardeny, Z. V. *Adv. Funct. Mater.* **2002**, *12*, 587–597.
(23) (a) Coropceanu, V.; Cornil, J.; da Silva Filho, D. A.; Olivier, Y.; Silbey, R.; Bredas, J.-L. *Chem. Rev.* **2007**, *107*, 926–952. (b) Babel, A.; Li, D.; Xia, Y.; Jenekhe, S. A. *Macromolecules* **2005**, *38*, 4705–4711.
(24) (a) Haskal, E. I.; Shen, Z.; Burrows, P. E.; Forrest, S. R. *Phys. Rev. B* **1995**, *51*, 4449–4462. (b) Yoffe, A. D. *Adv. Phys.* **1993**, *42*, 173–266.
(25) (a) Xin, H.; Kim, F. S.; Jenekhe, S. A. *J. Am. Chem. Soc.* **2008**, *130*, 5424–5425. (b) Xin, H.; Ren, G.; Kim, F. S.; Jenekhe, S. A. *Chem. Mater.* **2008**, *20*, 6199–6207.
(26) (a) Berson, S.; Bettignies, R. D.; Bailly, S.; Guillerez, S. *Adv. Funct. Mater.* **2007**, *17*, 1377–1384. (b) van Bavel, S. S.; Sourty, E.; de With, G.; Loos, J. *Nano Lett.* **2009**, *9*, 507–513.
(27) Briseno, A. L.; Mannsfeld, S. C. B.; Shamberger, P. J.; Ohuchi, F. S.; Bao, Z.; Jenekhe, S. A.; Xia, Y. *Chem. Mater.* **2008**, *20*, 4712–4719.
(28) (a) Zhu, Y.; Alam, M. M.; Jenekhe, S. A. *Macromolecules* **2003**, *36*, 8958–8968. (b) Chen, S. H.; Zhu, Y.; Jenekhe, S. A.; Su, A. C.; Chen, S. A. *J. Phys. Chem. B* **2007**, *111*, 12345–12350.
(29) Sze, S. M. *Physics of Semiconductor Devices*; Wiley: New York, 1981.
(30) Guo, X.; Kim, F. S.; Jenekhe, S. A.; Watson, M. D. *J. Am. Chem. Soc.* **2009**, *131*, 7206–7207.
(31) (a) Scharber, M. C.; Mühlbacher, D.; Koppe, M.; Denk, P.; Waldauf, C.; Heeger, A. J.; Brabec, C. J. *Adv. Mater.* **2006**, *18*, 789–794. (b) Cascio, A. J.; Lyon, J. E.; Beerbom, M. M.; Schlaf, R.; Zhu, Y.; Jenekhe, S. A. *Appl. Phys. Lett.* **2006**, *88*, 062104.
(32) (a) Blom, P. W. M.; Mihailetchi, V. D.; Koster, L. J. A.; Markov, D. E. *Adv. Mater.* **2007**, *19*, 1551–1566. (b) Mihailetchi, V. D.; Xie, H. X.; de Boer, B.; Koster, L. J. A.; Blom, P. W. M. *Adv. Funct. Mater.* **2006**, *16*, 699–708. (c) Moliton, A.; Nunzi, J.-M. *Polym. Int.* **2006**, *55*, 583–600.
(33) (a) Clarke, T. M.; Ballantyne, A. M.; Nelson, J.; Bradley, D. D. C.; Durrant, J. R. *Adv. Funct. Mater.* **2008**, *18*, 4029–4035. (b) Riedel, I.; Parisi, J.; Dyakonov, V.; Lusten, L.; Vanderzande, D.; Hummelen, J. C. *Adv. Funct. Mater.* **2004**, *11*, 38–44.
(34) Murgatroyd, P. N. *J. Phys. D: Appl. Phys* **1970**, *3*, 151–156.